Concordance of immunological events between intrarectal and intravenous $SHIV_{AD8-EO}$ infection when assessed by Fiebig-equivalent staging

Joana Dias,[1] Giulia Fabozzi,[2] Kylie March,[2] Mangaiarkarasi Asokan,[3] Cassandra G. Almasri,[3] Jonathan Fintzi,[4] Wanwisa Promsote,[1] Yoshiaki Nishimura,[5] John-Paul Todd,[6] Jeffrey D. Lifson,[7] Malcolm A. Martin,[5] Lucio Gama,[1] Constantinos Petrovas,[2] Amarendra Pegu,[3] John R. Mascola,[3] and Richard A. Koup[1]

[1]Immunology Laboratory, Vaccine Research Center, [2]Tissue Analysis Core, Vaccine Research Center, [3]Virology Laboratory, Vaccine Research Center, [4]Biostatistics Research Branch, [5]Laboratory of Molecular Biology, and [6]Translational Research Program, Vaccine Research Center, National Institute of Allergy and Infectious Diseases, National Institutes of Health, Bethesda, Maryland, USA. [7]AIDS and Cancer Virus Program, Leidos Biomedical Research Inc., Frederick National Laboratory for Cancer Research, Frederick, Maryland, USA.

Primary HIV-1 infection can be classified into six Fiebig stages based on virological and serological laboratory testing, whereas simian-HIV (SHIV) infection in nonhuman primates (NHPs) is defined in time post-infection, making it difficult to extrapolate NHP experiments to the clinics. We identified and extensively characterized the Fiebig-equivalent stages in NHPs challenged intrarectally or intravenously with $SHIV_{AD8-EO}$. During the first month post-challenge, intrarectally challenged monkeys were up to 1 week delayed in progression through stages. However, regardless of the challenge route, stages I–II predominated before, and stages V–VI predominated after, peak viremia. Decrease in lymph node (LN) $CD4^+$ T cell frequency and rise in $CD8^+$ T cells occurred at stage V. LN virus-specific $CD8^+$ T cell responses, dominated by degranulation and TNF, were first detected at stage V and increased at stage VI. A similar late elevation in follicular $CXCR5^+$ $CD8^+$ T cells occurred, consistent with higher plasma CXCL13 levels at these stages. LN $SHIV_{AD8-EO}$ RNA^+ cells were present at stage II, but appeared to decline at stage VI when virions accumulated in follicles. Fiebig-equivalent staging of $SHIV_{AD8-EO}$ infection revealed concordance of immunological events between intrarectal and intravenous infection despite different infection progressions, and can inform comparisons of NHP studies with clinical data.

Introduction

Early diagnosis of HIV-1 infection is crucial to interrupt viral transmission networks and initiate treatment in the earliest stages of infection. These early interventions may in turn reduce plasma viremia and set-point viral loads, slow down $CD4^+$ T cell depletion, improve HIV-specific T cell functions, and decrease the size of the latent reservoir (1, 2). Early diagnosis requires methods adapted to detect hallmarks of acute and early HIV-1 infection, as well as an adequate staging system that reflects the initial evolution of the infection and that may inform the course of disease.

Fiebig et al. (3) were the first to stage primary HIV-1 infection based on laboratory assays conducted in 435 plasma samples from 51 seroconverting donors. In that study, the authors defined 6 stages of primary HIV-1 infection, each of them characterized by a unique pattern of detection of different viral markers: HIV-1 RNA measured by quantitative PCR, HIV-1 p24 antigen measured by ELISA, and HIV antibodies measured by either third-generation IgM-sensitive ELISA or Western blot (3). Altogether, the plasma donors in that study transitioned from stage I (only HIV-1 RNA positive) to stage II (only HIV-1 RNA and p24 antigen positive), stage III (HIV RNA, p24 antigen, and HIV antibody ELISA positive, but Western blot negative), stage IV (HIV antibody ELISA positive but indeterminate Western blot), stage V (Western blot positive without p31 band), and stage VI (Western blot positive with p31 band) (3). This staging system has been widely used to stratify patient cohorts, meaningfully compare pathogenesis and clinical data, validate mathematic models of viral evolution, and assess the influence of early treatment interventions (4–12).

Nonhuman primate (NHP) models are a powerful resource to develop and test vaccine platforms as well as therapeutic strategies aimed at functional cure or eradication of HIV-1 infection (13). However, in contrast to HIV-1 infection, the progression of simian-HIV (SHIV) infection and timing of interventions being tested are usually indicated in *time post-infection* (14–22), making it a challenge to accurately extrapolate such strategies to human clinical settings. Given that the Fiebig stages are widely used to classify acute and early HIV-1 infection in humans, the mapping of equivalent stages in NHPs would thus be important for the extrapolation of therapeutic approaches from NHP models to HIV-infected humans.

In this study, we used virological and serological testing to identify the Fiebig-equivalent stages of infection in rhesus macaques challenged with $SHIV_{AD8-EO}$ via the intrarectal or intravenous route, and performed extensive immunological characterization of the different Fiebig-equivalent stages. Despite different kinetics of infection progression in intrarectally and intravenously

Conflict of interest: The authors have declared that no conflict of interest exists.

Submitted: May 21, 2021; **Accepted:** July 22, 2021; **Published:** September 1, 2021.
Reference information: *J Clin Invest*. 2021;131(17):e151632.
https://doi.org/10.1172/JCI151632.

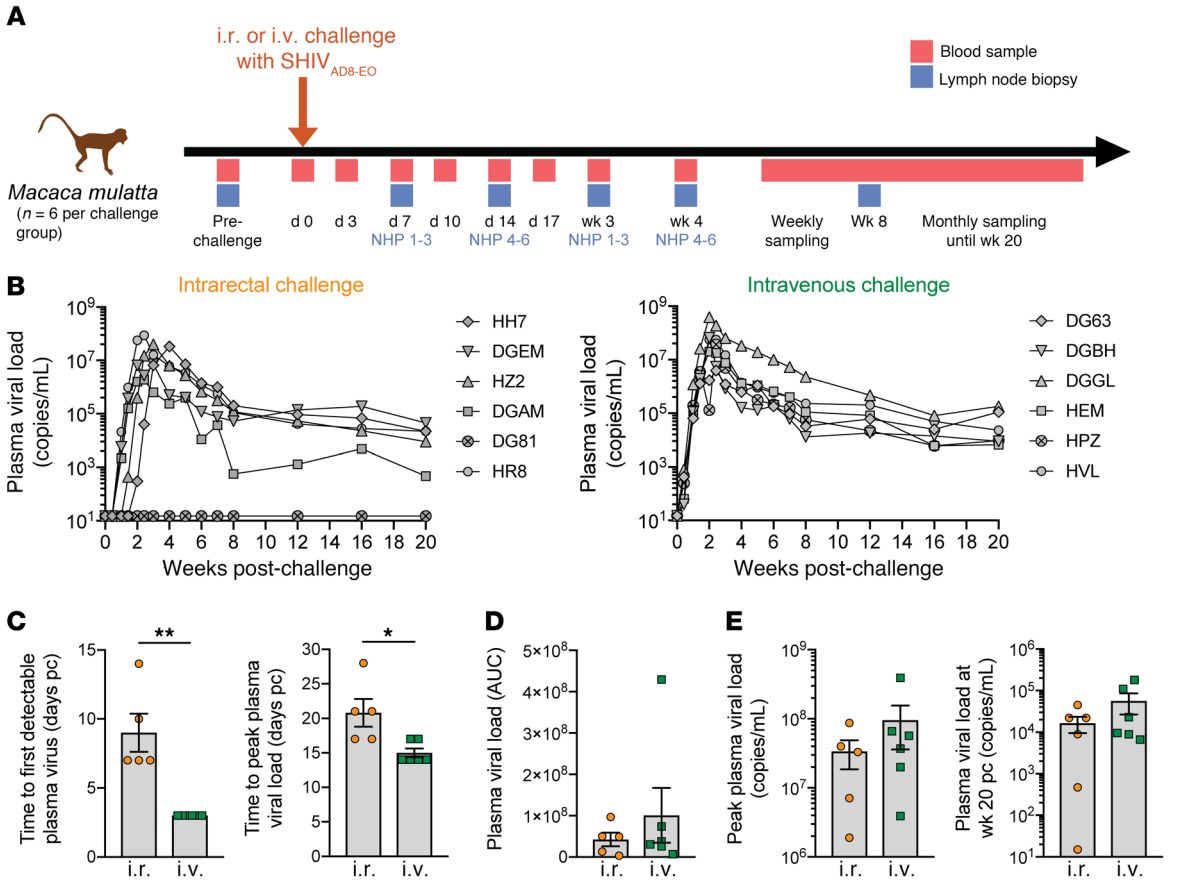

Figure 1. Study design and kinetics of $SHIV_{AD8-EO}$ infection in rhesus macaques. (**A**) Twelve rhesus macaques were challenged either intrarectally (n = 6) or intravenously (n = 6) with 1000 or 100 $TCID_{50}$ of $SHIV_{AD8-EO}$, respectively, and sampled at different time points during the course of the infection. The orange arrow indicates challenge with $SHIV_{AD8-EO}$, and the red and blue squares indicate time points of blood sampling and LN collection, respectively. (**B**) Plasma viral load up to 20 weeks post-challenge in the monkeys challenged with $SHIV_{AD8-EO}$ via the i.r. (left) or i.v. (right) route. (**C**) Time to first detectable plasma virus (left) and to peak plasma viremia (right) upon i.r. or i.v. challenge with $SHIV_{AD8-EO}$. (**D** and **E**) Plasma viral load throughout the first 20 weeks after $SHIV_{AD8-EO}$ challenge as determined by area under the curve (AUC) analysis (**D**), and at the peak time point (left) and 20 weeks post-challenge (right) (**E**). Bar graphs show the mean ± SEM and individual data points (**C**–**E**). The Mann-Whitney test was used to detect significant differences between each 2 groups with unpaired samples (**C**–**E**). *P < 0.05; **P < 0.01. i.r., intrarectal; i.v., intravenous; NHP, nonhuman primate; pc, post-challenge.

$SHIV_{AD8-EO}$-challenged monkeys, systemic immunological events such as the development of simian immunodeficiency virus–specific (SIV-specific) $CD8^+$ T cell responses and detection of virus-producing cells and virions in the lymph nodes (LNs) were concordant between the challenge groups when evaluated by Fiebig-equivalent staging.

Results

The rate and kinetics of $SHIV_{AD8-EO}$ infection varied with the challenge route. To map and characterize the Fiebig-equivalent stages of $SHIV_{AD8-EO}$ infection, Indian-origin rhesus macaques were inoculated either intrarectally (n = 6) or intravenously (n = 6) with $SHIV_{AD8-EO}$ at previously reported challenge doses: 1000 and 100 median tissue culture infective doses ($TCID_{50}$) of $SHIV_{AD8-EO}$, respectively (17, 23). Peripheral blood samples and LN biopsies were collected at different time points throughout the first 5 months post-challenge (Figure 1A). As each animal could only be biopsied up to 4 times, each subgroup of 3 animals followed a different LN biopsy schedule (Figure 1A) in order to maximize the number of samples obtained in the early stages of infection.

We initially compared the intrarectal (i.r.) and intravenous (i.v.) challenge routes in terms of infection rate and kinetics. Plasma virus was detected in 5 of 6 intrarectally challenged monkeys, whereas all 6 intravenously challenged monkeys became infected (Figure 1B). Long-term follow-up of monkey DG81 did not reveal any plasma virus up to 39 weeks post-challenge, which suggests that this monkey never became infected. Plasma virus was first detected 7–14 days post-challenge in the intrarectally challenged monkeys, and significantly earlier at 3 days post-challenge in all intravenously challenged monkeys (P = 0.002; Figure 1C, left). Furthermore, the time to reach peak plasma viral load was significantly longer in the monkeys challenged via the i.r. route compared with the i.v. route (ranges 17–28 days vs. 14–17 days, respectively, P = 0.02; Figure 1C, right). Despite these differences, the overall plasma viral load as measured by area under the curve (Figure 1D) as well as the peak and set-point viral loads (Figure 1E) did not vary significantly with the challenge route. Overall, these data reveal differences in the infection rate and kinetics between the challenge groups not reflected by the plasma viral burden.

A

Time point (pc)	d 0	d 3	d 7	d 10	d 14	d 17	wk 3	wk 4	wk 5	wk 6	wk 7	wk 8	wk 12	wk 16	wk 20
Intrarectal challenge															
HH7	-	Eclipse	Eclipse	Eclipse	I	I	II	V	V	VI	VI	VI	VI	VI	VI
DGEM	-	Eclipse	I	I	II	IV	V	V	VI	VI	VI	VI	VI	VI	VI
HZ2	-	Eclipse	Eclipse	I	I	II	III	V	V	V	VI	VI	VI	VI	VI
DGAM	-	Eclipse	I	I	II	II	V	V	VI	VI	VI	VI	VI	VI	VI
HR8	-	Eclipse	I	I	II	III	V	VI	VI	VI	VI	VI	VI	VI	VI
DG81	-	-	-	-	-	-	-	-	-	-	-	-	-	-	-
Intravenous challenge															
DG63	-	I	I	II	II	III	V	V	V	V	VI	VI	VI	VI	ND
DGBH	-	I	I	II	II	III	V	V	VI	VI	VI	VI	VI	VI	
DGGL	-	I	II	II	II	IV	V	V	V	V	VI	VI	VI	VI	
HEM	-	I	I	II	II	V	V	V	V	VI	VI	VI	VI	VI	
HPZ	-	I	I	II	II	V	V	VI	VI	VI	VI	VI	VI	VI	
HVL	-	I	I	II	III	III	V	VI	VI	VI	VI	VI	VI	VI	

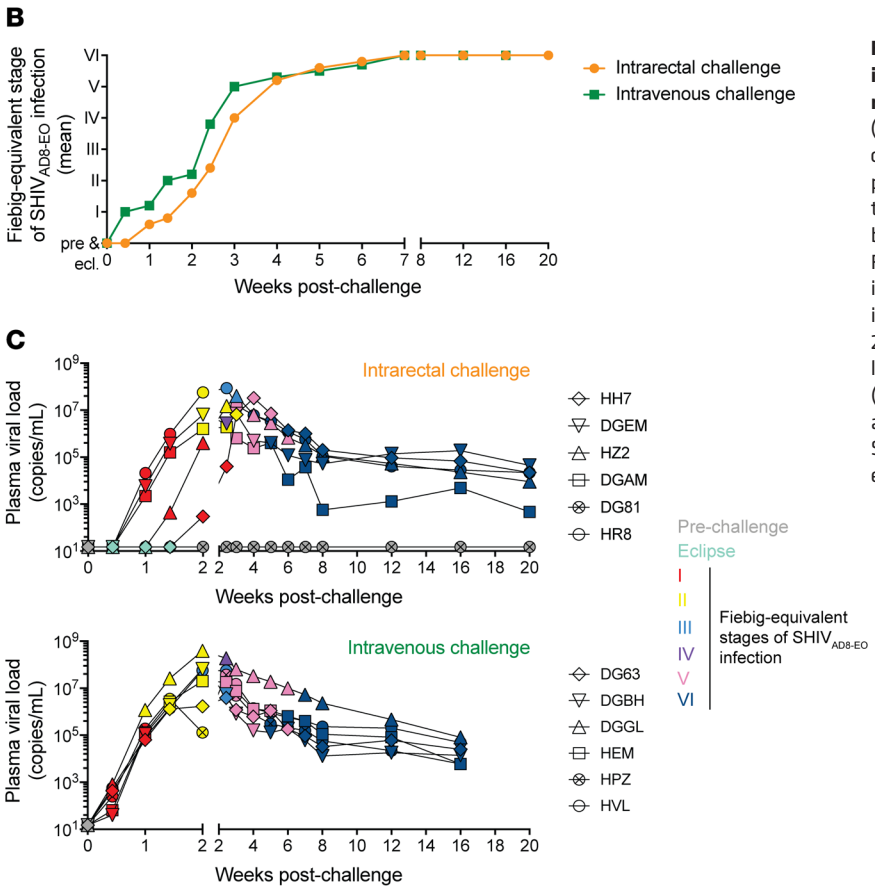

Figure 2. Fiebig-equivalent stages of infection in monkeys challenged intrarectally or intravenously with $SHIV_{AD8\text{-}EO}$. (**A**) Map of the Fiebig-equivalent stages of $SHIV_{AD8\text{-}EO}$ infection up to 20 weeks post-challenge in monkeys challenged via the i.r. or i.v. route. (**B**) Correspondence between time post-challenge and mean Fiebig-equivalent stage of $SHIV_{AD8\text{-}EO}$ infection in monkeys challenged via the i.r. or i.v. route. (**C**) Plasma viral load up to 20 weeks post-challenge in monkeys challenged with $SHIV_{AD8\text{-}EO}$ via the i.r. (top) or i.v. (bottom) route. Each data point is colored according to the Fiebig-equivalent stage of $SHIV_{AD8\text{-}EO}$ infection at that time point. ecl., eclipse; ND, not determined.

The pattern of Fiebig-equivalent stages of $SHIV_{AD8\text{-}EO}$ infection varied with the challenge route during the first 4 weeks post-challenge. The Fiebig stages of HIV-1 infection are defined by unique patterns of detection of virus RNA, p24 antigen, and HIV antibodies by either ELISA or Western blot (3). To define the Fiebig-equivalent stages of $SHIV_{AD8\text{-}EO}$ infection, we adapted HIV plasma tests to SHIV (Supplemental Table 1; supplemental material available online with this article; https://doi.org/10.1172/JCI151632DS1) and performed them on plasma samples from the intrarectally and intravenously challenged monkeys. The tests included quantitative reverse transcription PCR to detect plasma SIV Gag RNA (Supplemental Figure 1A), ELISAs to detect either SIV p27 antigen (Supplemental Figure 1B) or antibodies against HIV-1/HIV-2 (Supplemental Figure 1C), and Western blot assays to detect SIV Gag and Pol antibodies (Supplemental Figure 2A) and HIV Env antibodies (Supplemental Figure 2B and Supplemental Table 1). Integration of results from these tests as previously described (3) allowed us to map the Fiebig-equivalent stages over the course of 16–20 weeks of $SHIV_{AD8\text{-}EO}$ infection (Table 1 and Figure 2A).

At day 3 post-challenge, all intrarectally challenged monkeys were still in the eclipse phase, whereas the intravenously challenged monkeys had already entered Fiebig-equivalent stage I (Figure 2A). All viremic animals progressed through Fiebig-equivalent stages I and II, which were more synchronized in the intravenously challenged monkeys (Figure 2A), consistent with less variation in time to first detect plasma virus within this group (Figure 1C). Fiebig-equivalent stage III was detected between weeks 2 and 3 post-challenge in only 5 of the 11 viremic monkeys (Fig-

Table 1. Laboratory assay results defining the Fiebig-equivalent stages of $SHIV_{AD8-EO}$ infection, and duration of stages in $SHIV_{AD8-EO}$ infection and HIV-1 infection

Stages	Fiebig-equivalent stages of $SHIV_{AD8-EO}$ infection								Fiebig stages of HIV-1 infection (3)	
	Viral markers (laboratory assay)				Individual duration in days (95% CI)		Time to reach stages in days (95% CI)		Duration in days (95% CI)	
	SIV Gag RNA (qRT-PCR)	SIV p27 antigen (ELISA)	HIV-1/HIV-2 antibodies (IgM-sensitive ELISA)	SIV and HIV antibodies (Western blots)	i.r. challenge	i.v. challenge	i.r. challenge	i.v. challenge	Individual	Cumulative
I	+	–	–	–	8 (7, 9)	6 (5, 7)	4 (3, 5)	3 (2, 4)	5.0 (3.1, 8.1)	5.0 (3.1, 8.1)
II	+	+	–	–	7 (5, 9)	5 (4, 6)	12 (11, 14)	9 (8, 10)	5.3 (3.7, 7.7)	10.3 (7.1, 13.5)
III	+	+	+	–	3 (2, 5)	2 (1, 4)	19 (17, 23)	14 (13, 15)	3.2 (2.1, 4.8)	13.5 (10.0, 17.0)
IV	+	+[A]	+	I					5.6 (3.8, 8.1)	19.1 (15.3, 22.9)
V	+	+/–	+	+[B]	13 (8, 17)	17 (10, 24)	23 (20, 25)	17 (15, 18)	69.5 (39.7, 121.7)	88.6 (47.4, 129.8)
VI	+	+/–	+	+[C]	Open-ended	Open-ended	35 (30, 42)	34 (27, 41)	Open-ended	Open-ended

I, indeterminate Western blot lacking reactivity to 2 of the following 3 bands: p27, gp41, g120/g160. i.r., intrarectal; i.v., intravenous. [A]Fiebig stage IV of HIV-1 infection is characterized by the presence or absence of HIV-1 p24 antigen (3). Of the only 2 samples in this study at Fiebig-equivalent stage IV, SIV p27 was detected in both. [B]Without p31 band. [C]With p31 band.

ure 2A). While all intrarectally challenged animals had entered Fiebig-equivalent stage V or VI by week 4, 2 of the 6 intravenously challenged animals entered stage V as early as 17 days post-challenge, and they were followed 4 days later by the remaining animals (Figure 2A). Overall, NHPs challenged via the i.r. route had an up to 1-week delay in progression through Fiebig-equivalent stages during the first 4 weeks post-challenge when compared with NHPs challenged via the i.v. route (Figure 2B). The multistate model (MSM) estimated that the average rate of progression for early stage transitions up to Fiebig-equivalent stage V among intravenously challenged animals was 1.3 (95% CI: 1.2, 1.7) times the rate of progression among intrarectally challenged animals. The initial faster progression through Fiebig-equivalent stages in the i.v. group is consistent with the faster kinetics of $SHIV_{AD8-EO}$ infection in these animals (Figure 1C). The average rate of progression from Fiebig-equivalent stage V to VI among intravenously challenged animals was 0.7 (95% CI: 0.4, 1.4) times the rate of progression among intrarectally challenged animals, and, by week 7, all monkeys had entered Fiebig-equivalent stage VI, independent of the challenge route (Figure 2A). In conclusion, the pattern of Fiebig-equivalent stages of $SHIV_{AD8-EO}$ infection differed between the challenge groups during the first 4 weeks post-challenge. Table 1 summarizes the expected days spent in each stage and the expected time until each stage is reached. Notably, week 12 and week 16 post-challenge samples from aviremic monkey DG81 gave rise to a low positive signal in the anti–HIV-1/2 antibody ELISA (Supplemental Figure 1), possibly due to matrix effects from sample components and/or cross-reactivity between plate-bound recombinant HIV-1/2 antigens and other antibodies in the samples.

Combination of plasma viral load data and staging of $SHIV_{AD8-EO}$ infection revealed that, regardless of the challenge route, Fiebig-equivalent stages I to II predominated during the period of time preceding peak viremia, whereas stages V and VI predominated after peak viremia had been reached (Figure 2C). This pattern is in agreement with the set of viral markers that defines each stage (Table 1). Thus, despite the observed differences in stage synchronization and pace of progression between the groups, the Fiebig-equivalent stages of $SHIV_{AD8-EO}$ infection predominating before and after peak viremia were similar in both challenge groups.

Plasma levels of CXCL13 increased during the course of $SHIV_{AD8-EO}$ infection. We further characterized the cytokine and chemokine profile of Fiebig-equivalent stages of $SHIV_{AD8-EO}$ infection. Plasma samples from the intrarectally and intravenously challenged monkeys from day 0 (pre-challenge) to week 20 post-challenge were analyzed using Luminex technology and standard ELISA. The sample selection allowed a fair representation of all Fiebig-equivalent stages of infection (Figure 3A) except for stage IV, which was identified in only 2 monkeys at day 17 post-challenge (Figure 2). Higher levels of the proinflammatory cytokine IL-8 were detected in some monkeys at Fiebig-equivalent stages I to III (Figure 3, B and C). Moreover, the levels of IL-15 were significantly upregulated at Fiebig-equivalent stage II when compared with pre-challenge ($P = 0.004$), eclipse phase ($P < 0.001$), stage I ($P = 0.01$), stage V ($P = 0.01$), and stage VI ($P = 0.001$; Figure 3, B and D). Also, the levels of monocyte chemoattractant protein-1 (MCP-1) were significantly higher at Fiebig-equivalent stage II than pre-challenge and at stage I of infection ($P = 0.01$ for both comparisons; Figure 3, B and E). Interestingly, no other significant differences were detected in the levels of Th1, Th2, and Treg cytokines across stages. Next, we investigated the levels of CXCL13, a chemokine involved in the migration of B cells and T follicular helper (Tfh) cells to the lymphoid follicles (24–27), whose serum levels were reportedly elevated in HIV-infected subjects (28). Plasma CXCL13 levels were significantly higher at Fiebig-equivalent stages III, V, and VI compared with pre-challenge ($P = 0.02$, $P < 0.001$, and $P < 0.001$, respectively), eclipse ($P = 0.03$,

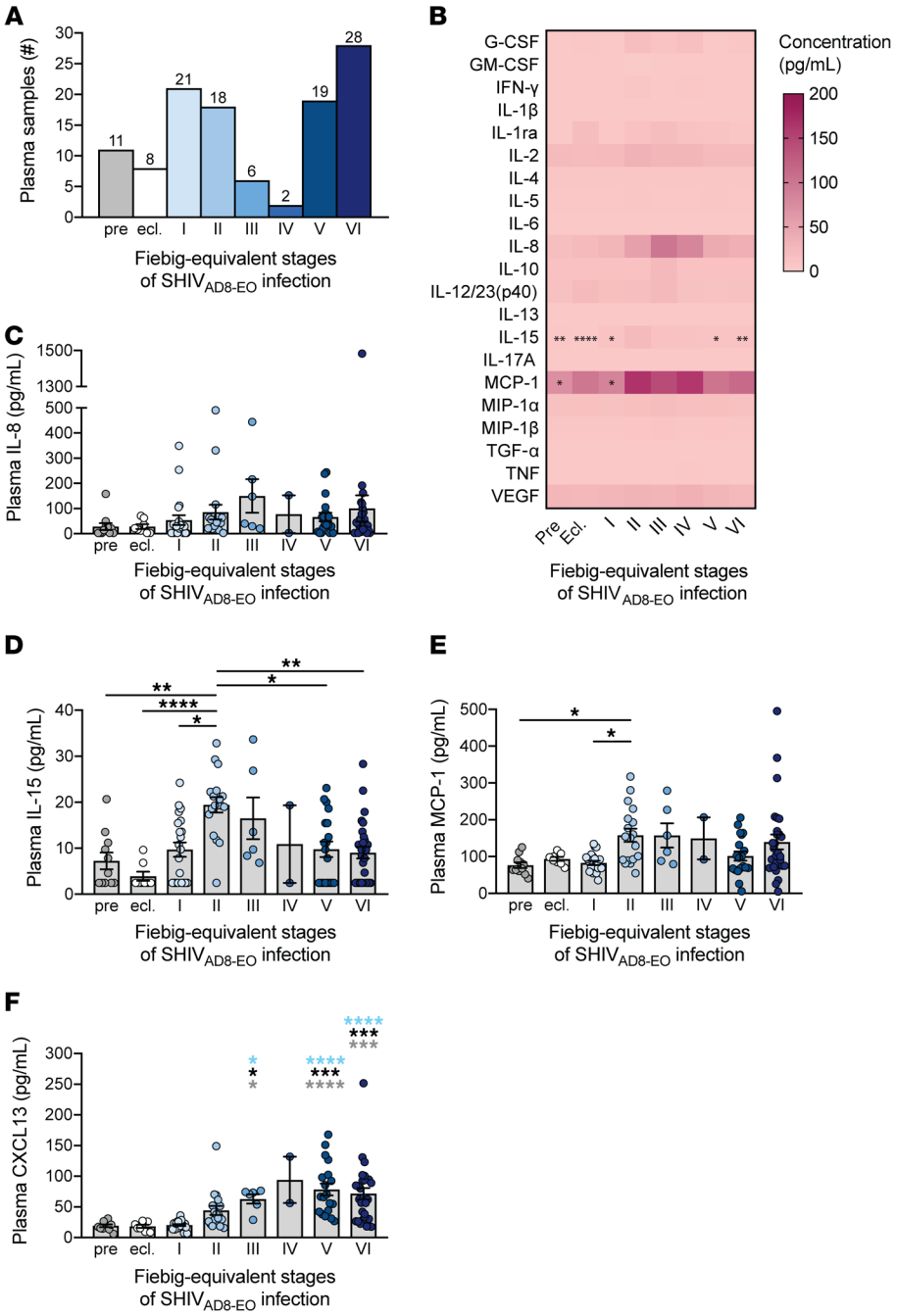

Figure 3. Cytokine and chemokine profile of the Fiebig-equivalent stages of $SHIV_{AD8\text{-}EO}$ infection. (**A**) Distribution of plasma samples for cytokine and chemokine analysis across the Fiebig-equivalent stages of $SHIV_{AD8\text{-}EO}$ infection. (**B**) Heatmap depicting median plasma cytokine and chemokine levels in each stage of $SHIV_{AD8\text{-}EO}$ infection, as determined in a bead-based multiplex assay using Luminex technology. (**C**–**E**) Plasma levels of IL-8 (**C**), IL-15 (**D**), and MCP-1 (**E**) in each stage of $SHIV_{AD8\text{-}EO}$ infection, as measured by Luminex. (**F**) Plasma levels of CXCL13 in each stage of $SHIV_{AD8\text{-}EO}$ infection, as measured by ELISA. Bar graphs show the absolute number (**A**), and the mean ± SEM and individual data points (**C**–**F**). The Kruskal-Wallis test followed by Dunn's multiple-comparison test was used to detect significant differences between all stages except for Fiebig-equivalent stage IV (low *n*) (**B**–**F**). The statistical results indicate significant differences between those stages and Fiebig-equivalent stage II (**B**), and statistical results denoted in gray, black, and blue reflect comparisons with the pre-challenge phase, eclipse phase, and Fiebig-equivalent stage I, respectively (**F**). $^{*}P < 0.05$; $^{**}P < 0.01$; $^{***}P < 0.001$; $^{****}P < 0.0001$. ecl., eclipse.

$P < 0.001$, and $P < 0.001$, respectively), and stage I ($P = 0.01$, $P < 0.001$, and $P < 0.001$, respectively) of infection (Figure 3F). Overall, these data show a transient increase of IL-15 and MCP-1 levels at Fiebig-equivalent stage II and higher CXCL13 levels during Fiebig-equivalent stages III, V, and VI of $SHIV_{AD8\text{-}EO}$ infection in rhesus macaques.

Frequency of LN CD8⁺ T cells increased at Fiebig-equivalent stages V and VI of $SHIV_{AD8\text{-}EO}$ infection. Since CXCL13 is involved in the redirection of B and Tfh cells to lymphoid follicles, we studied the dynamics of several immune cell populations throughout the course of $SHIV_{AD8\text{-}EO}$ infection in LN biopsy samples. With the exception of Fiebig-equivalent stage IV, all remaining stages were represented in the collection of LN samples (Figure 4A). LN cells were stained for markers that allowed flow cytometry identification of T cells, B cells, natural killer (NK) cells, and monocytes (Supplemental Figure 3A). Overall, the levels of these cell populations remained relatively stable during the course of $SHIV_{AD8\text{-}EO}$ infection, and only a transient increase in NK cell levels at Fiebig-equivalent stage V was detected ($P = 0.02$ for stage V vs. stage II or VI; Figure 4B). As expected, the levels of $CD4^+$ T cells significantly decreased at Fiebig-equivalent stages V and VI ($P = 0.03$ and $P = 0.003$ for pre-challenge vs. stage V or VI, respectively), which was accompanied by an increase in the levels of $CD8^+$ T cells (pre-challenge vs. stage V, $P = 0.05$; pre-challenge vs. stage VI, $P = 0.006$; and stage II vs. stage VI, $P = 0.05$) (Figure 4C). These changes in the LNs occurred despite stable cell subset levels in PBMCs (Supplemental Figure 3, B–D). For a better assessment of T cell dynamics within the LNs, we included markers to identify germinal center (GC) Tfh cells ($CD95^{hi}CXCR5^+PD\text{-}1^{hi}$ $CD4^+$ T cells) and follicular $CD8^+$ (fCD8⁺) T cells ($CCR7^{lo}CD95^{hi}CXCR5^{hi}$ $CD8^+$ T cells), as previously described (refs. 29–31 and Supplemental Figure 3A). While GC Tfh cells remained relatively stable across Fiebig-equivalent stages, higher levels were observed in some animals at stage VI, consistent with earlier studies reporting accumulation of Tfh cells during chronic SIV/HIV infection (32–34). In

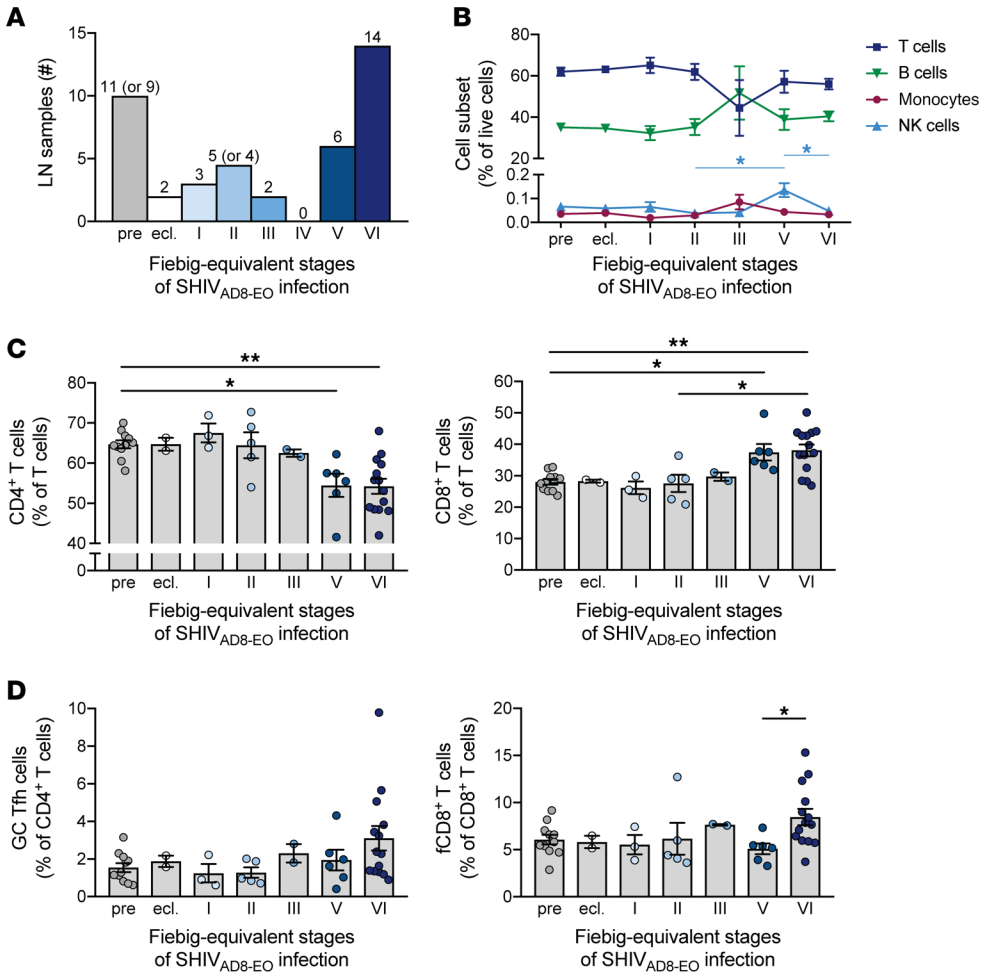

Figure 4. Immune cell distribution in the LNs throughout the Fiebig-equivalent stages of SHIV$_{AD8-EO}$ infection. (**A**) Average distribution of LN samples for flow cytometry immunophenotyping analysis (shown in Figure 4) and CD8$^+$ T cell functional analysis (shown in Figure 5) across the Fiebig-equivalent stages of SHIV$_{AD8-EO}$ infection (the numbers in parentheses indicate the number of samples available for the functional analysis shown in Figure 5 when the sample number was different from that for the immunophenotyping analysis shown in Figure 4). (**B**–**D**) Frequency of monocytes, NK cells, B cells, and T cells (**B**), CD4$^+$ (left) and CD8$^+$ (right) T cells (**C**), and GC Tfh (left) and fCD8$^+$ T cells (right) (**D**) at the different stages of SHIV$_{AD8-EO}$ infection. Graphs show the mean (**A**), the mean ± SEM (**B**), and the mean ± SEM and individual data points (**C** and **D**). The Kruskal-Wallis test followed by Dunn's multiple-comparison test was used to detect significant differences between the pre-challenge phase, Fiebig-equivalent stages II, V, and VI of SHIV$_{AD8-EO}$ infection (**B**–**D**). *P < 0.05; **P < 0.01. ecl., eclipse; fCD8$^+$, follicular CD8$^+$; GC, germinal center; Tfh, T follicular helper.

addition, fCD8$^+$ T cells slightly increased at stage VI (P = 0.05; Figure 4D). Taken together, these data indicate that the frequency of LN CD8$^+$ T cells increases during Fiebig-equivalent stages V and VI of SHIV$_{AD8-EO}$ infection.

LN SIV Gag–specific CD8$^+$ T cell responses developed at Fiebig-equivalent stages V and VI of SHIV$_{AD8-EO}$ infection. We next investigated in which stage of infection SIV-specific CD8$^+$ T cell responses are generated in the LNs. LN cells were stimulated for 6 hours with SIV Gag peptide pool, and CD8$^+$ T cells were then evaluated for production of cytokines (IFN-γ, MIP-1β, and TNF) and degranulation (through CD107a expression) by flow cytometry (Figure 5A and Supplemental Figure 3E). Similar to the immunophenotyping experiments (Figure 4), we used samples from all Fiebig-equivalent stages but stage IV, and only slightly fewer samples from the pre-challenge phase and stage II (Figure 4A). SIV-specific CD8$^+$ T cells, defined as CD8$^+$ T cells expressing CD107a or coexpressing CD69 with IFN-γ, TNF, or MIP-1β, were predominantly detected at the late Fiebig-equivalent stages V and VI of SHIV$_{AD8-EO}$ infection (P = 0.002 and P = 0.02 for stage VI vs. pre-challenge or stage II, respectively; Figure 5B). We conducted polyfunctionality analysis using SPICE software to dissect whether CD107a expression, which dominated the CD8$^+$ T cell response at Fiebig-equivalent stage VI (Figure 5C), occurred alone or in combination with cytokine production. The dominant CD8$^+$ T cell response was monofunctional CD107a expression at Fiebig-equivalent stage VI, whereas it was either monofunctional CD107a or monofunctional TNF at Fiebig-equivalent stage V (P = 0.003 for pie chart comparison; Figure 5D). CD8$^+$ T cells expressing CD107a alone or in combination with TNF were detected at significantly higher levels in stage VI than stage V (P = 0.01 and P = 0.03, respectively; Figure 5E). In conclusion, SIV Gag–specific CD8$^+$ T cell responses developed mostly in Fiebig-equivalent stages V and VI of SHIV$_{AD8-EO}$ infection with a distinct profile in each of the stages.

SHIV$_{AD8-EO}$ RNA$^+$ virions accumulated in LN follicles during Fiebig-equivalent stages V and VI of SHIV$_{AD8-EO}$ infection. Finally, we investigated the presence and localization of SHIV$_{AD8-EO}$ RNA in the LNs at each Fiebig-equivalent stage of SHIV$_{AD8-EO}$ infection. LN sections from all but Fiebig-equivalent stage IV were stained using RNAscope in situ hybridization technology (ref. 35 and Figure 6, A and B), and the numbers of SHIV$_{AD8-EO}$ RNA$^+$ cells and SHIV$_{AD8-EO}$ RNA$^+$ virions were quantified at each stage of infection. In order to rule out any influence of the size of the LN sections in the quantification, the absolute numbers of viral RNA$^+$ cells and virions were normalized to the LN areas, which, nonetheless, did not vary considerably across stages (Supplemental Figure 4A). SHIV$_{AD8-EO}$ RNA$^+$ cells were initially detected at stage II of infection, and their levels appeared to decline in most monkeys at stage VI, although the difference did not reach statistical significance (Figure 6C, left). In contrast, few SHIV$_{AD8-EO}$ RNA$^+$ virions were detected at stage II, but their levels increased

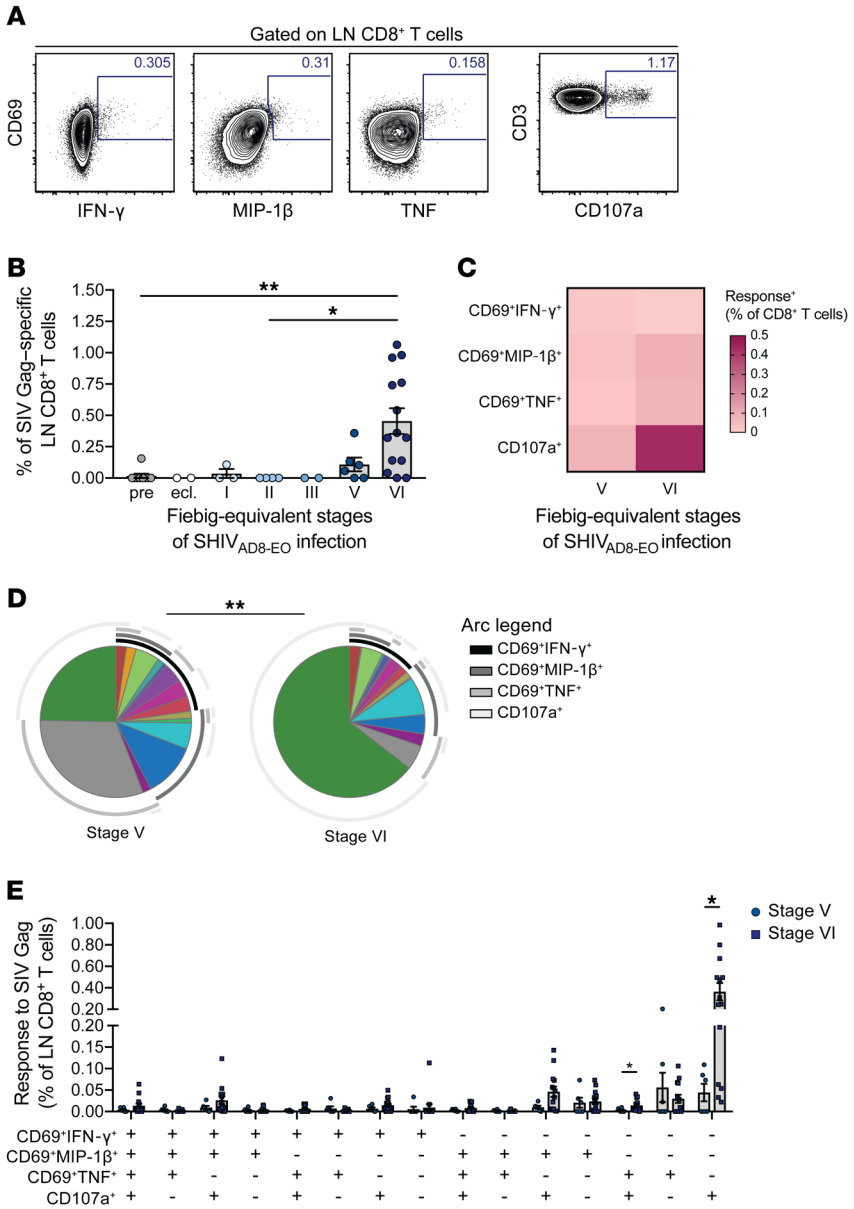

Figure 5. LN SIV Gag–specific CD8⁺ T cell responses across the Fiebig-equivalent stages of $SHIV_{AD8-EO}$ infection. (**A**) Representative example of the coexpression of CD69 and IFN-γ, MIP-1β, or TNF, as well as of CD107a expression, by CD8⁺ T cells from the LNs of $SHIV_{AD8-EO}$-challenged monkeys, after 6 hours of stimulation with SIV Gag peptide pool. (**B**) Frequency of LN CD8⁺ T cells either coexpressing CD69 and IFN-γ, MIP-1β, or TNF, or expressing CD107a, in each stage of $SHIV_{AD8-EO}$ infection, after SIV Gag peptide pool–mediated stimulation. (**C**) Heatmap depicting the median frequency of LN CD8⁺ T cells expressing each functional readout in Fiebig-equivalent stages V and VI of $SHIV_{AD8-EO}$ infection, after 6 hours of stimulation with SIV Gag peptide pool. (**D** and **E**) Polyfunctional profile of LN CD8⁺ T cells in response to SIV Gag peptide pool in Fiebig-equivalent stages V and VI of $SHIV_{AD8-EO}$ infection. The pie charts and bar plot show the frequency of CD8⁺ T cells expressing all different combinations of functional readouts. Bar graphs show the mean ± SEM and individual data points (**B** and **E**), and pie charts show the mean frequency of responding CD8⁺ T cells (**D**). The Kruskal-Wallis test followed by Dunn's multiple-comparison test was used to detect significant differences between the prechallenge phase, Fiebig-equivalent stages II, V, and VI of $SHIV_{AD8-EO}$ infection (**B**). The permutation test and the Mann-Whitney test were used to compare the pie charts (**D**) and data in the bar plot (**E**), respectively. $*P < 0.05$; $**P < 0.01$. ecl., eclipse.

thereafter and remained relatively stable up to stage VI of infection (Figure 6C, right). Overall, the levels of $SHIV_{AD8-EO}$ RNA⁺ cells in the LNs strongly correlated with plasma viremia (Spearman's $r = 0.8571$, $P < 0.0001$) (Supplemental Figure 4B), but did not correlate with the frequency of SIV Gag–specific LN CD8⁺ T cells either producing cytokines or degranulating (Spearman's $r = 0.1260$, $P = 0.4$; Supplemental Figure 4C), or simply degranulating (Spearman's $r = 0.09325$, $P = 0.6$; Supplemental Figure 4D) in response to SIV Gag peptide pool.

To determine where in the LNs the $SHIV_{AD8-EO}$ RNA⁺ cells and virions were located, the same parameters were analyzed in the follicular and extrafollicular areas (defined by the presence or lack of CD20 expression, respectively). $SHIV_{AD8-EO}$ RNA⁺ cells and virions were detected in both follicular and extrafollicular areas, although in different patterns (Figure 6, A, D, and E). While, in median, less than half of the $SHIV_{AD8-EO}$ RNA⁺ cells were detected in the follicles throughout $SHIV_{AD8-EO}$ infection (median percentage of follicular $SHIV_{AD8-EO}$ RNA⁺ cells: 30.10%, 33.92%, and 36.81% at stages II, V, and VI, respectively), $SHIV_{AD8-EO}$ RNA⁺ virions preferentially accumulated in the follicles at stages V and VI of infection (median percentage of follicular $SHIV_{AD8-EO}$ RNA⁺ virions: 30.16%, 63.17%, and 85.37% at stages II, V, and VI, respectively; $P = 0.001$ for follicular vs. extrafollicular virion load at stage VI), where they were found associated with the follicular dendritic cell network (Figure 6, A, D, and E). Importantly, these results were not influenced by the size of the follicular and extrafollicular areas nor by the number of follicles, which remained relatively stable across the Fiebig-equivalent stages of $SHIV_{AD8-EO}$ infection (Supplemental Figure 4, E–G).

Collectively, these data indicate distinct patterns of detection of $SHIV_{AD8-EO}$ RNA⁺ cells and virions in the LNs of $SHIV_{AD8-EO}$-infected macaques, whereby $SHIV_{AD8-EO}$ RNA⁺ cells may predominate earlier in infection while $SHIV_{AD8-EO}$ RNA⁺ virions accumulate later and mostly in the follicles.

Discussion

The existence of a viral infection staging system that can be used in parallel in animal models and patients is critical to accurately extrapolate preclinical novel therapeutic interventions to potential clinical application. In the HIV field, the Fiebig staging system (3) has been extensively used to inform

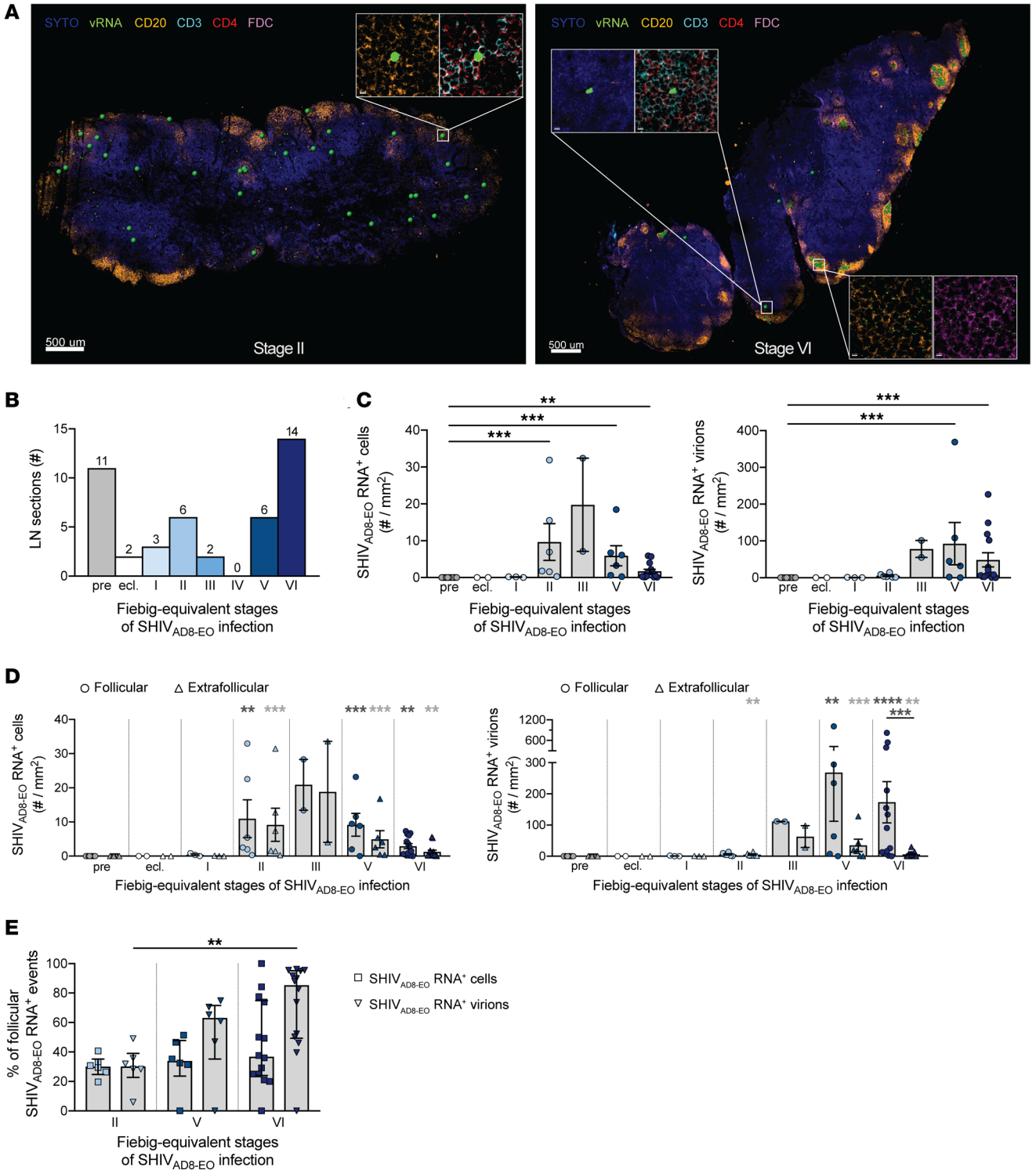
A
SYTO vRNA CD20 CD3 CD4 FDC
500 um
Stage II
SYTO vRNA CD20 CD3 CD4 FDC
500 um
Stage VI
B
LN sections (#)
11
2
3
6
2
0
6
14
pre ecl. I II III IV V VI
Fiebig-equivalent stages of SHIV AD8-EO infection
C
SHIV AD8-EO RNA+ cells (# / mm2)
pre ecl. I II III V VI
Fiebig-equivalent stages of SHIV AD8-EO infection
SHIV AD8-EO RNA+ virions (# / mm2)
pre ecl. I II III V VI
Fiebig-equivalent stages of SHIV AD8-EO infection
D
Follicular
Extrafollicular
SHIV AD8-EO RNA+ cells (# / mm2)
pre ecl. I II III V VI
Fiebig-equivalent stages of SHIV AD8-EO infection
Follicular
Extrafollicular
SHIV AD8-EO RNA+ virions (# / mm2)
pre ecl. I II III V VI
Fiebig-equivalent stages of SHIV AD8-EO infection
E
% of follicular SHIV AD8-EO RNA+ events
II V VI
Fiebig-equivalent stages of SHIV AD8-EO infection
SHIV AD8-EO RNA+ cells
SHIV AD8-EO RNA+ virions

Figure 6. Detection of $SHIV_{AD8-EO}$ RNA in LN tissues by RNAscope. (**A**) Representative staining of LN sections (scale bars: 500 μm) from Fiebig-equivalent stages II (left) and VI (right) of $SHIV_{AD8-EO}$ infection, showing cellular nucleic acids (SYTO, blue), $SHIV_{AD8-EO}$ RNA (green), CD20 (yellow), CD3 (turquoise), CD4 (red), and FDC network (pink). $SHIV_{AD8-EO}$ RNA^+ cells and virions are marked with large and small green spheres, respectively. Insets (scale bars: 5 μm) show a magnified view of $SHIV_{AD8-EO}$ RNA^+ cells associated with CD3, CD4, and CD20 (stage II, top right), CD3 and CD4 (stage VI, top left); and of follicular virions associated with the FDC network (stage VI, bottom right). Insets show the real $SHIV_{AD8-EO}$ RNA signal. (**B**) Distribution of LN sections for RNAscope analysis across Fiebig-equivalent stages of $SHIV_{AD8-EO}$ infection. (**C** and **D**) RNAscope quantification of $SHIV_{AD8-EO}$ RNA^+ cells and virions across whole LN sections (**C**) and in LN follicular (circles) and extrafollicular (triangles) areas (**D**) in each stage of infection. (**E**) Percentage of follicular $SHIV_{AD8-EO}$ RNA^+ cells (squares) and virions (triangles) at stages II, V, and VI of infection. Bar graphs show the absolute numbers (**B**), and individual data points with the mean ± SEM (**C** and **D**) or median and interquartile range (**E**). The Kruskal-Wallis test followed by Dunn's multiple-comparison test was used to detect significant differences in viral parameters between pre-challenge, stages II, V, and VI of infection in the whole LN tissue (**C**), follicular areas (dark gray, **D**), and extrafollicular areas (light gray, **D**), as well as in the percentage of follicular $SHIV_{AD8-EO}$ RNA^+ cells or virions between stages II, V, and VI (**E**). Statistical results in gray reflect differences from the pre-challenge phase (**D**). The Mann-Whitney test was used to compare viral parameters between follicular and extrafollicular areas (**D**). $^{**}P < 0.01$; $^{***}P < 0.001$; $^{****}P < 0.0001$. ecl., eclipse; FDC, follicular dendritic cell; vRNA, viral RNA.

about HIV-1 disease progression and stratify patient cohorts in clinical trials, but a parallel system in NHPs, widely used to develop vaccination and therapeutic strategies, is lacking. In this study, we delineated the Fiebig-equivalent stages of infection in NHPs challenged intrarectally or intravenously with $SHIV_{AD8-EO}$, and extensively characterized them immunologically. Progression through Fiebig-equivalent stages during the first 4 weeks post-challenge was overall up to 1 week delayed in monkeys challenged via the i.r. route compared with the i.v. route (Figure 2). However, regardless of the challenge group, Fiebig-equivalent stages I–II and V–VI predominated before and after plasma peak viremia, respectively (Figure 2). In contrast to the stable immune cell distribution observed in peripheral blood, a decrease in the frequency of $CD4^+$ T cells and concomitant rise in the frequency of $CD8^+$ T cells in the LNs occurred at Fiebig-equivalent stage V of infection. SIV-specific $CD8^+$ T cell responses developed after peak viremia at Fiebig-equivalent stages V and VI, when $SHIV_{AD8-EO}$ RNA^+ cells appeared to decline and virions accumulated in the follicles (Figure 7). Overall, we found concordance of immunological events between monkeys challenged via the i.r. and i.v. route when evaluated by Fiebig-equivalent staging, despite differences in progression of $SHIV_{AD8-EO}$ infection between the challenge groups.

To our knowledge, this is the first report that maps the stages of SHIV infection in NHPs based on the Fiebig stages of HIV-1 infection in humans (3). We showed that the Fiebig-equivalent staging pattern varied with the challenge route during the first 4 weeks post-challenge, such that intrarectally challenged monkeys were overall up to 1 week delayed in stage progression when compared with intravenously challenged monkeys. This delay is consistent with the significantly longer time that it took to first detect plasma viremia and for viremia to peak in intrarectally challenged monkeys, and may be partially explained by the need for local viral expansion at the initial site of infection before systemic dissemination, as previously reported (36–38). Thus, in acute infection studies in NHPs, describing the timing of interventions in days or weeks post-infection can be imprecise, as these may correspond to different Fiebig-equivalent stages depending on the challenge route. If such studies are to be extrapolated to human clinical trials, they should indicate in what Fiebig-equivalent stage their interventions were initiated. In this context, Nishimura et al. (17, 39) showed long-term control of infection in approximately half of the monkeys that were challenged intrarectally or intravenously with $SHIV_{AD8-EO}$ and given broadly neutralizing antibodies (bNAbs) starting as early as day 3 or day 14 post-challenge. According to our findings, these results mean that bNAb therapies can be successful if initiated within the eclipse phase or Fiebig-equivalent stages I and II. As these stages occur before viral control begins and antibodies arise, collectively, these data support the hypothesis that this early bNAb intervention may lead to the formation of immune complexes that will ultimately alter cellular immune responses (17). These data may also suggest that, to be effective, bNAb interventions need to be initiated before viral dissemination and establishment of a long-lived, persistent, and rebound-competent viral reservoir. Comparison of stages between $SHIV_{AD8-EO}$ and HIV-1 infection (Table 1) shows that, on average, Fiebig-equivalent stage VI starts earlier in NHPs because of a much shorter Fiebig-equivalent stage V of $SHIV_{AD8-EO}$ infection compared with the counterpart Fiebig stage V of HIV-1 infection (average 13 and 17 days in the i.r. and i.v. NHP groups, respectively, vs. 69.5 days in HIV-1–infected subjects) (3). Thus, our findings also have important implications for interventions aiming at the earlier phases of Fiebig stage VI (recent infection and early chronic infection) (3, 40), as they will have to be initiated much earlier in NHPs in order to target a similar phase of disease progression in humans.

Immunological characterization of the Fiebig-equivalent stages of $SHIV_{AD8-EO}$ infection showed that, despite the observed differences in progression of infection between the challenge groups, the timing of virus-specific $CD8^+$ T cell responses, as well as the viral load and virus distribution in the LNs, was concordant between the groups when assessed by Fiebig-equivalent staging. LN $SHIV_{AD8-EO}$ RNA^+ cells were initially detected in both follicular and extrafollicular areas and mostly preceding peak plasma viremia at Fiebig-equivalent stage II, in agreement with previous studies (31, 41–44). Their levels increased proportionally to viral load in plasma, and seemed to decrease at Fiebig-equivalent stage VI when strong LN SIV-specific $CD8^+$ T cell responses were detected. These responses, which appeared to develop at later stages than in the peripheral blood of acutely HIV-1–infected subjects (45), were predominantly characterized by production of the highly proinflammatory cytokine TNF and expression of CD107a, indicative of degranulation. In addition, levels of fCD8+ T cells, previously shown to be highly cytolytic ex vivo and able to mediate killing of HIV-infected target cells in vitro (31, 46), were higher at Fiebig-equivalent stage VI than stage V. LN NK cell levels also transiently increased at Fiebig-equivalent stage V. Thus, our data are consistent with the notion that, after peak plasma viremia during Fiebig-equivalent

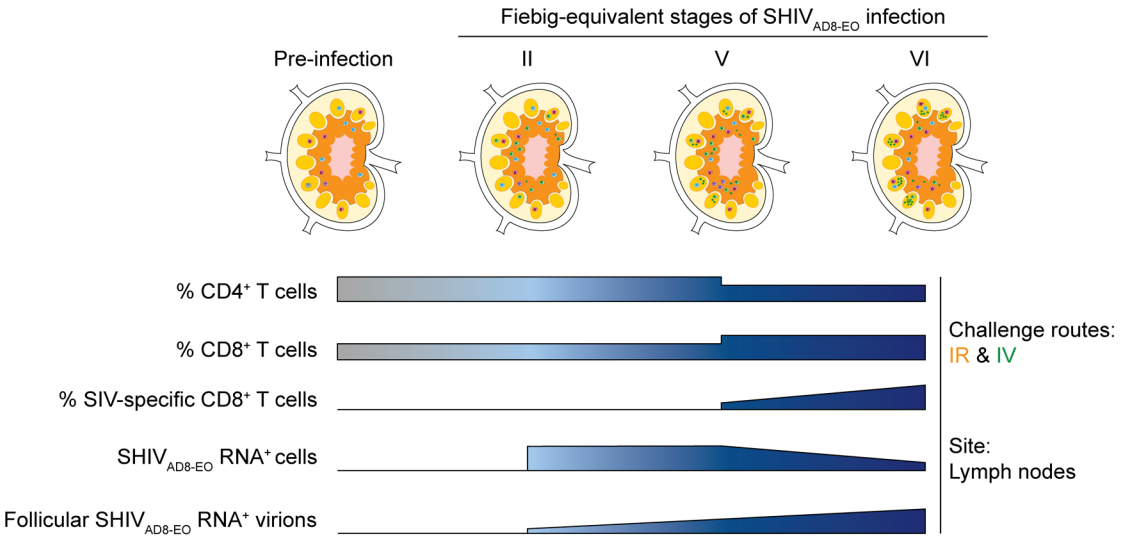

Figure 7. Schematic characterization of the Fiebig-equivalent stages of SHIV$_{AD8-EO}$ infection in rhesus macaques. Summary illustration of changes occurring in the lymph nodes during the Fiebig-equivalent stages of infection in monkeys challenged with SHIV$_{AD8-EO}$ via the i.r. or i.v. route. The big and small green spheres in the lymph node pictures at stages II, V, and VI represent virus-infected cells and virions, respectively. i.r., intrarectal; i.v., intravenous.

stages V and VI of SHIV$_{AD8-EO}$ infection, cytotoxic immune responses develop in the LNs and may lead to lysis of virus-infected cells and release of virions. In fact, LN SHIV$_{AD8-EO}$ RNA$^+$ virions were almost absent at Fiebig-equivalent stage II when SHIV$_{AD8-EO}$ RNA$^+$ cells, likely producing virions (47), were already present but CD8$^+$ T cell responses were undetectable. However, virions were highly abundant in the follicles during Fiebig-equivalent stage VI when CD8$^+$ T cell responses were stronger. Although there was no significant correlation between the levels of LN SHIV$_{AD8-EO}$ RNA$^+$ cells and the virus-specific function of LN CD8$^+$ T cells in our study, possibly because of limited sample size and data variation between animals, previous studies reported in situ observation of CD8$^+$ T cells expressing T cell intracellular antigen-1 (TIA-1) or perforin (48, 49) and increased activation of cytotoxic cells (50) in the LNs of HIV-1–infected subjects. Furthermore, CD8$^+$ T cells with HIV- or SIV-specific killing activity in vitro were detected in the LNs, splenic white pulp, and tonsil GCs of HIV-1–infected subjects (46, 51), and in the LNs of SIV-infected NHPs (31, 52, 53). Also, NK cells were shown to accumulate in the LNs of African green monkeys during nonpathogenic SIV infection, where they played an important role in the control of viral replication (54).

It is noteworthy that the staging pattern and the associated immunological characteristics reported here are only valid for the virus and challenge routes that we have studied, and it is possible that other viruses and routes do not follow the same timing and immunological patterns. In relation to this, it was perhaps surprising that we did not detect throughout the Fiebig-equivalent stages of SHIV$_{AD8-EO}$ infection significant changes from baseline in the plasma levels of cytokines and chemokines (with the exception of IL-15, MCP-1, and CXCL13), and in the peripheral blood levels of CD4$^+$ T cells. It is possible that the SHIV$_{AD8-EO}$ stock used in this study played a significant role in this regard, as 1 of 12 challenged monkeys in our study (monkey DG81) did not appear to have been infected with this virus stock. In addition, previous studies showed changes not only in IL-15 and MCP-1 levels, but also in MIP-1α, IFN-γ, TNF, IL-1β, and IL-1Ra, among others, early in HIV-1 infection and pathogenic SIVmac251 progressive infection (55–57). However, such changes were much more attenuated upon infection with hepatitis B virus (55) or with either nonprogressive or nonpathogenic SIV strains (57). The other possibility is that, because these parameters were evaluated very early after infection (up to 20 weeks post-challenge), not enough time had passed to allow detection of changes in peripheral blood. Intrarectal or intravenous infection of rhesus macaques with different doses of SHIV$_{AD8-EO}$ led to a rapid decrease of CD4$^+$ T cell frequency in the bronchoalveolar lavage fluid within the first 20 weeks post-challenge, similar to what we have observed in LNs, but depletion of CD4$^+$ T cells from peripheral blood, as evaluated by absolute cell counts, occurred rather gradually in most of the animals throughout a 100-week observation period (58). Notably, we reported frequencies of CD4$^+$ T cells out of total T cells, and absolute CD4$^+$ T cell counts would be required to truly assess whether CD4$^+$ T cell depletion has occurred, as previously reported in untreated HIV-1–infected patients in Fiebig stages II–IV compared with stage I (6). Muir et al. (59) also showed a decrease in the frequency of circulating resting memory B cells during early acute HIV-1 infection. Although the total B cell population remained relatively stable in our study, a more detailed B cell–oriented analysis would be required to evaluate the dynamics of this cell population throughout the Fiebig-equivalent stages of SHIV$_{AD8-EO}$ infection.

In summary, we mapped the Fiebig-equivalent stages in rhesus macaques challenged intrarectally or intravenously with SHIV$_{AD8-EO}$, and showed that, despite early variation in progression of infection and staging pattern with the challenge route, there is concordance in immunological events between the groups when evaluated by Fiebig-equivalent staging. Given the importance of the macaque model in HIV research, the definition and characterization of these stages will be useful to efficiently design new therapeutic strategies and accurately extrapolate them to the clinics.

Methods

Study design

Twelve Indian-origin, outbred, young adult female and male rhesus macaques (*Macaca mulatta*) that did not express the MHC class I alleles *Mamu-A*01*, *Mamu-B*08*, and *Mamu-B*17*, associated with spontaneous virological control, were housed at BIOQUAL Inc. The animals were challenged either intrarectally (n = 6) or intravenously (n = 6) with 1000 or 100 median tissue culture infective doses ($TCID_{50}$) of $SHIV_{AD8\text{-}EO}$, respectively, as previously described (23). The origin and preparation of the tissue culture–derived $SHIV_{AD8\text{-}EO}$ stock have been previously reported (58). Challenge animal groups were balanced for FcγRII and FcγRIII genotypes. Blood samples for plasma and peripheral blood mononuclear cell (PBMC) isolation were taken biweekly during the first 3 weeks post-challenge, then weekly up to week 8 post-challenge, and monthly thereafter (Figure 1A). In each group, LN biopsies were collected at 4 time points: pre-challenge (n = 6, left inguinal LNs), day 7 (n = 3) or day 14 (n = 3) (right inguinal LNs), week 3 (n = 3) or week 4 (n = 3) (left axillary LNs), and week 8 (n = 6, right axillary LNs; Figure 1A). The intermediate LN time points were staggered to increase the number of samples from early stages of $SHIV_{AD8\text{-}EO}$ infection, given that each animal could only be biopsied up to 4 times.

Tissue processing

PBMCs were isolated from peripheral blood by Ficoll-Hypaque density gradient centrifugation (Sigma-Aldrich), frozen in FBS (Gibco) with 10% DMSO (Sigma-Aldrich), and stored in liquid nitrogen until further use. Plasma was isolated and immediately stored in aliquots at –80°C. To obtain LN cell suspensions, fat and connective tissue surrounding the LN were removed, and the tissue was then cut into small pieces and dissociated with the plastic end of a 6 mL syringe plunger. Cell suspensions were filtered through a 40 μm cell strainer, washed twice in RPMI 1640 medium supplemented with 10% FBS, 2 mM L-glutamine, 100 U/mL penicillin, and 100 μg/mL streptomycin (all from Gibco) (complete medium), then frozen in FBS with 10% DMSO, and stored in liquid nitrogen until required.

Plasma viral loads

Plasma viremia was quantitated through an established quantitative reverse transcription PCR (qRT-PCR) assay that quantifies SIV Gag RNA levels with a detection limit of 15 copies/mL, as previously described (60).

Detection of SIV p27 antigen, HIV antibodies, and SIV antibodies

ELISAs for detection of plasma SIV p27 antigen (ABL Inc.) and HIV-1/HIV-2 antibodies (third-generation IgM-sensitive ELISA, Abnova), as well as Western blot overnight assays for detection of plasma SIV and HIV antibodies using nitrocellulose strip–based kits (ZeptoMetrix Corp. and MP Biomedicals, respectively), were performed per the manufacturer's instructions. The Western blot strips were imaged using the G:BOX Mini 9 system and GeneSys software version 1.6.3.0 (Syngene). Data from the qRT-PCR, ELISAs, and Western blots were integrated as previously described (3) to identify the Fiebig-equivalent stages of $SHIV_{AD8\text{-}EO}$ infection (Supplemental Table 1).

Soluble cytokine and chemokine analyses

Plasma levels of 21 cytokines and chemokines were measured using the Luminex technology in a bead-based multiplex assay (MilliporeSigma), and CXCL13 levels were quantitated using a human CXCL13 ELISA (R&D Systems), both according to the manufacturer's instructions.

Functional assays

LN SIV-specific $CD8^+$ T cell responses were evaluated by in vitro peptide pool stimulation against SIV Gag. Thawed LN cells were rested for 1 hour at 37°C/5% CO_2 in complete medium, and then incubated for 6 hours with either 4 μg/mL SIV Gag peptide pool (NIH AIDS Reagent Program, Manassas, Virginia, USA) or DMSO (vehicle, unstimulated control) in the presence of monensin (GolgiStop, BD Biosciences) and brefeldin A (Sigma-Aldrich) as well as anti-CD107a antibody (clone H4A3, BioLegend) to determine cellular degranulation. For each functional readout, the residual response levels of the unstimulated cells were subtracted from the response levels of the SIV Gag–stimulated cells.

Flow cytometry

For phenotypic analyses, thawed cells were stained with Zombie UV amine reactive dye (BioLegend) and then with directly conjugated antibodies against surface markers for 15 minutes at room temperature (RT). Cells were washed in PBS containing 2% FBS (FACS buffer) and fixed in 1% paraformaldehyde before data acquisition. For functional analyses, cells were incubated with Aqua amine reactive dye (Invitrogen), surface-stained with directly conjugated and biotinylated antibodies for 15 minutes at RT, and then incubated with streptavidin (BioLegend) for 15 minutes at RT. FACS buffer was used to wash cells in between and right after each incubation step. This was followed by cell fixation and permeabilization in Cytofix/Cytoperm (BD Biosciences) for 30 minutes at 4°C, washes in Perm/Wash buffer (BD Biosciences), and intracellular staining with directly conjugated antibodies for 30 minutes at 4°C. Cells were then washed in Perm/Wash buffer and resuspended in FACS buffer for data acquisition. The antibodies were used at predetermined optimal titers and are listed in Supplemental Table 2. Samples were acquired on a modified BD FACSymphony (BD Biosciences) equipped with 355-, 405-, 488-, 532-, and 628-nm lasers, and data were analyzed using FlowJo software version 9.9.6 (BD Biosciences). Polyfunctionality analyses were performed using Simple Presentation of Incredibly Complex Evaluations (SPICE) software version 6.0 (Mario Roederer, Vaccine Research Center, National Institute of Allergy and Infectious Diseases, NIH).

$SHIV_{AD8\text{-}EO}$ RNA detection in LN tissues

After biopsy, residual fat was removed from the LNs, which were then fixed overnight at RT in PBS 1× containing 4% paraformaldehyde (Electron Microscopy Science) and embedded in paraffin blocks. Tissue sections of 5 μm thickness were mounted on SuperFrost slides (Thermo Fisher Scientific) and subjected to RNAscope analysis (Advanced Cell Diagnostics). Briefly, slides were baked for 1 hour at 60°C, deparaffinized twice in xylene (5 minutes each), and dehydrated twice in ethanol bath (2 minutes each). Slides were then treated with hydrogen peroxide for 10 minutes at RT, rinsed in deionized water, and incubated in antigen retrieval buffer for 15 minutes at 100°C using a steamer. Slides were then immediately treated with RNAscope®Protease Plus (Advanced Cell Diagnostics) for 15 minutes at 40°C in a HybEZ hybridization oven (Advanced Cell Diagnostics).

Hybridization with $SHIV_{AD8-EO}$ pooled probe spanning *gag-pol* (20ZZ, targeting the region 2184–3342) and *vif-vpu-nef* (34ZZ, targeting the region 2–751 nt) occurred for 2 hours at 40°C and was followed by the amplification steps per the RNAscope Multiplex Fluorescent V2 assay protocol, and the TSA-FITC (1:1500; PerkinElmer) detection step.

After RNAscope, staining of B cells ($CD20^+$), T cells ($CD3^+CD4^+$), and the follicular dendritic cell (FDC) network was performed for confocal microscopy. Specifically, after 1 hour of incubation with blocking solution (PBS 1×, 0.3% Triton X-100, 1% BSA), primary unconjugated antibodies directed against CD3 (clone F7.2.38, Dako) and FDC (clone CNA.42, Sigma-Aldrich) were added on the slides overnight at 4°C. After 3 washing steps (in PBS 1× at RT for 15 minutes each), slides were incubated for 2 hours at RT with fluorescently conjugated donkey anti-mouse IgG1a (Alexa Fluor 594 conjugated, Thermo Fisher Scientific) and goat anti-mouse IgM (Alexa Fluor 546 conjugated, Thermo Fisher Scientific) to detect CD3 and FDC, respectively. After 3 washing steps, slides were blocked with 10% normal mouse/goat serum for 1 hour at RT and incubated with directly conjugated antibodies against CD20 (clone L26, eFluor 660 conjugated, eBioscience) and CD4 (goat polyclonal antibody, Alexa Fluor 700 conjugated, catalog FAB8165N, R&D Systems) for 2 hours at RT. After 3 additional washing steps, slides were counterstained for nuclear staining with Syto40 (1:100,000; Thermo Fisher Scientific) for 40 minutes at RT, mounted with Prolong Gold Antifade (Thermo Fisher Scientific), and allowed to cure for over 24 hours in the dark.

Tissues were imaged using a Nikon C2 confocal microscope (×40 objective, 1.40 NA), and images were processed using Imaris version 9.5.0 (Bitplane). Using Imaris's built-in function Spots, $SHIV_{AD8-EO}$ RNA^+ cells and $SHIV_{AD8-EO}$ RNA^+ virions were identified and quantified. The Spots function identifies fluorescent signals based on a defined diameter and subsequently marks them with a green sphere (large or small for $SHIV_{AD8-EO}$ RNA^+ cells and $SHIV_{AD8-EO}$ RNA^+ virions, respectively) for easier visualization. For $SHIV_{AD8-EO}$ RNA^+ cells, a diameter of 7 μm was assigned based on previous literature that established 7.5 μm as the average cell diameter (61, 62), and on the average calculated diameter from randomly selected $SHIV_{AD8-EO}$ RNA^+ cells across our studies. For the $SHIV_{AD8-EO}$ RNA^+ virions, a diameter of 2 μm was assigned based on the average measured virus particle RNAscope signal diameter from across our studies. Any background artifacts that were identified by the Spots function were manually excluded by 2 independent individuals based on (a) size and shape of the virus RNA^+ staining, (b) presence of the virus RNA^+ staining on at least 3 confocal optical planes, and/or (c) highly saturated nuclear Syto40 fluorescence. Data were normalized by area (mm^2) to take into account differences in tissue size.

Statistics

Statistical comparison of challenge groups or Fiebig-equivalent stages of $SHIV_{AD8-EO}$ infection. Statistical analyses were performed using Prism software version 8 (GraphPad). For comparison of 2 groups with unpaired samples, the nonparametric Mann-Whitney test was used. For comparison of more than 2 groups with unpaired samples, the Kruskal-Wallis test was used and followed by Dunn's multiple-comparison test when the Kruskal-Wallis *P* value was significant. The permutation test in the SPICE software was used to compare the pie charts depicting polyfunctionality data. Correlations were assessed using Spearman's rank correlation test. Two-sided *P* values less than 0.05 without further adjustment for multiple comparisons were considered significant.

Multistate model for progression of $SHIV_{AD8-EO}$ infection. A multistate model (MSM) for progression of $SHIV_{AD8-EO}$ infection in rhesus macaques based on the Fiebig-equivalent stages of infection was developed. The input data for the model consisted of the Fiebig-equivalent stages of $SHIV_{AD8-EO}$ infection recorded at increments of 3–7 days for each of 11 NHPs challenged intrarectally ($n = 5$) or intravenously ($n = 6$) with $SHIV_{AD8-EO}$ (Figure 2A). All animals start at stage 0, which corresponds to the eclipse phase. Owing to the limited sample size, subsequent stages were lumped as follows: A = {0}, B = {I}, C = {II}, D = {III, IV}, E = {V}, and F = {VI}. The model is a progressive time-homogeneous continuous-time multistate Markov model in which animals start in stage A, progress through the various stages, B through E, and finally reach stage F. Waiting times between transitions were assumed to be exponentially distributed with rate parameters λ_{AB}, λ_{BC}, λ_{CD}, and λ_{DE}. Because of the size of the data set, the effect of the challenge route was constrained to be the same across the first 4 transitions (A→B, B→C, C→D, D→E) via a log-linear model for the transition intensity. The effect of the challenge route on the rate of progression from E to F was allowed to differ from the effect on earlier transitions. Letting Z_i be an indicator for whether the challenge was i.v., the transition intensities for animal *i* were written as follows: $\log(\lambda_{AB}) = \beta_{AB} + \beta_1 Z_i$; $\log(\lambda_{BC}) = \beta_{BC} + \beta_1 Z_i$; $\log(\lambda_{CD}) = \beta_{CD} + \beta_1 Z_i$; $\log(\lambda_{DE}) = \beta_{DE} + \beta_1 Z_i$; and $\log(\lambda_{EF}) = \beta_{EF} + \beta_2 Z_i$, where β_{AB}, β_{BC}, β_{CD}, β_{DE}, and β_{EF} are the log transition intensities in the i.r. group, $\exp(\beta_1)$ is the common effect of i.v. challenge on early progression (common hazard ratio), and $\exp(\beta_2)$ is the effect of the challenge route on late progression. Confidence intervals for model estimates were calculated from quantiles of 1000 bootstrap samples. The bootstrap procedure resamples individual animals and was stratified on challenge route to preserve the number of animals per challenge group. The model was fit using the msm package in R (63, 64).

Study approval

All animal procedures and experiments were reviewed and approved by the Institutional Animal Care and Use Committee of the Vaccine Research Center (VRC), National Institute of Allergy and Infectious Diseases (NIAID), NIH.

Author contributions

JD, MA, MAM, LG, AP, JRM, and RAK designed the research. JD, GF, KM, CGA, WP, YN, and JPT performed the experiments. JF performed the computational modeling. JD, GF, KM, MA, CGA, JF, JDL, LG, CP, AP, and RAK analyzed the data. JD and RAK wrote the manuscript.

Acknowledgments

This work was supported by the Bill and Melinda Gates Foundation (grant OPP1147555) and by the Intramural Research Program of the VRC, NIAID, NIH. This work was also supported in part with federal funds from the National Cancer Institute, NIH, under contracts HHSN261200800001E and 75N91019D00024. We thank Elizabeth McCarthy, Hana Bao, Saran Bao, Jumugal Noor, Alida Taylor, and Diana Scorpio from the Translational Research Program, VRC, for support with the animal experiments, Mario Roederer from the ImmunoTechnology Section,

VRC, for flow cytometry advice, and David R. Ambrozak, Richard Nguyen, Erica Smit, Esther Thang, and Steve Perfetto from the Flow Cytometry Core, VRC, for help with the flow cytometers. We also thank the staff of the Quantitative Molecular Diagnostics Core of the AIDS and Cancer Virus Program, Leidos Biomedical Research Inc., Frederick National Laboratory for Cancer Research, for plasma viral load analyses. LN pictures in Figure 7 were generated using templates from the Biomedical PowerPoint Toolkit Suite, Motifolio Inc.

Address correspondence to: Richard A. Koup, Vaccine Research Center, National Institutes of Health, 40 Convent Drive, Bethesda, Maryland 20892, USA. Phone: 301.594.8585; Email: rkoup@mail.nih.gov.

1. O'Brien M, Markowitz M. Should we treat acute HIV infection? *Curr HIV/AIDS Rep*. 2012;9(2):101–110.
2. Smith MK, et al. The detection and management of early HIV infection: a clinical and public health emergency. *J Acquir Immune Defic Syndr*. 2013;63(suppl 2):S187–S199.
3. Fiebig EW, et al. Dynamics of HIV viremia and antibody seroconversion in plasma donors: implications for diagnosis and staging of primary HIV infection. *AIDS*. 2003;17(13):1871–1879.
4. Lee HY, et al. Modeling sequence evolution in acute HIV-1 infection. *J Theor Biol*. 2009;261(2):341–360.
5. Ananworanich J, et al. Impact of multi-targeted antiretroviral treatment on gut T cell depletion and HIV reservoir seeding during acute HIV infection. *PLoS One*. 2012;7(3):e33948.
6. Ananworanich J, et al. Virological and immunological characteristics of HIV-infected individuals at the earliest stage of infection. *J Virus Erad*. 2016;2(1):43–48.
7. Ananworanich J, et al. HIV DNA set point is rapidly established in acute HIV infection and dramatically reduced by early ART. *EBioMedicine*. 2016;11:68–72.
8. Ananworanich J, et al. Viral kinetics in untreated versus treated acute HIV infection in prospective cohort studies in Thailand. *J Int AIDS Soc*. 2017;20(1):21652.
9. Colby DJ, et al. Rapid HIV RNA rebound after antiretroviral treatment interruption in persons durably suppressed in Fiebig I acute HIV infection. *Nat Med*. 2018;24(7):923–926.
10. Dong KL, et al. Detection and treatment of Fiebig stage I HIV-1 infection in young at-risk women in South Africa: a prospective cohort study. *Lancet HIV*. 2018;5(1):e35–e44.
11. Peluso MJ, et al. Liver function test abnormalities in a longitudinal cohort of Thai individuals treated since acute HIV infection. *J Int AIDS Soc*. 2020;23(1):e25444.
12. Paci P, et al. Timely HAART initiation may pave the way for a better viral control. *BMC Infect Dis*. 2011;11:56.
13. Del Prete GQ, Lifson JD. Nonhuman primate models for studies of AIDS virus persistence during suppressive combination antiretroviral therapy. *Curr Top Microbiol Immunol*. 2018;417:69–109.
14. Hessell AJ, et al. Early short-term treatment with neutralizing human monoclonal antibodies halts SHIV infection in infant macaques. *Nat Med*. 2016;22(4):362–368.
15. Shapiro MB, et al. Single-dose bNAb cocktail or abbreviated ART post-exposure regimens achieve tight SHIV control without adaptive immunity. *Nat Commun*. 2020;11(1):70.
16. Bolton DL, et al. Human immunodeficiency virus type 1 monoclonal antibodies suppress acute simian-human immunodeficiency virus viremia and limit seeding of cell-associated viral reservoirs. *J Virol*. 2016;90(3):1321–1332.
17. Nishimura Y, et al. Early antibody therapy can induce long-lasting immunity to SHIV. *Nature*. 2017;543(7646):559–563.
18. Barouch DH, et al. Therapeutic efficacy of potent neutralizing HIV-1-specific monoclonal antibodies in SHIV-infected rhesus monkeys. *Nature*. 2013;503(7475):224–228.
19. Shingai M, et al. Antibody-mediated immunotherapy of macaques chronically infected with SHIV suppresses viraemia. *Nature*. 2013;503(7475):277–280.
20. Julg B, et al. Virological control by the CD4-binding site antibody N6 in simian-human immunodeficiency virus-infected rhesus monkeys. *J Virol*. 2017;91(16):e00498–00417.
21. Borducchi EN, et al. Antibody and TLR7 agonist delay viral rebound in SHIV-infected monkeys. *Nature*. 2018;563(7731):360–364.
22. Mavigner M, et al. Persistence of virus reservoirs in ART-treated SHIV-infected rhesus macaques after autologous hematopoietic stem cell transplant. *PLoS Pathog*. 2014;10(9):e1004406.
23. Shingai M, et al. Passive transfer of modest titers of potent and broadly neutralizing anti-HIV monoclonal antibodies block SHIV infection in macaques. *J Exp Med*. 2014;211(10):2061–2074.
24. Ansel KM, et al. A chemokine-driven positive feedback loop organizes lymphoid follicles. *Nature*. 2000;406(6793):309–314.
25. Allen CD, et al. Germinal-center organization and cellular dynamics. *Immunity*. 2007;27(2):190–202.
26. Breitfeld D, et al. Follicular B helper T cells express CXC chemokine receptor 5, localize to B cell follicles, and support immunoglobulin production. *J Exp Med*. 2000;192(11):1545–1552.
27. Schaerli P, et al. CXC chemokine receptor 5 expression defines follicular homing T cells with B cell helper function. *J Exp Med*. 2000;192(11):1553–1562.
28. Widney DP, et al. Serum levels of the homeostatic B cell chemokine, CXCL13, are elevated during HIV infection. *J Interferon Cytokine Res*. 2005;25(11):702–706.
29. Xu H, et al. PD-1(HIGH) follicular CD4 T helper cell subsets residing in lymph node germinal centers correlate with B cell maturation and IgG production in rhesus macaques. *Front Immunol*. 2014;5:85.
30. Velu V, et al. Induction of Th1-biased T follicular helper (Tfh) cells in lymphoid tissues during chronic simian immunodeficiency virus infection defines functionally distinct germinal center Tfh cells. *J Immunol*. 2016;197(5):1832–1842.
31. Ferrando-Martinez S, et al. Accumulation of follicular CD8+ T cells in pathogenic SIV infection. *J Clin Invest*. 2018;128(5):2089–2103.
32. Petrovas C, et al. CD4 T follicular helper cell dynamics during SIV infection. *J Clin Invest*. 2012;122(9):3281–3294.
33. Lindqvist M, et al. Expansion of HIV-specific T follicular helper cells in chronic HIV infection. *J Clin Invest*. 2012;122(9):3271–3280.
34. Perreau M, et al. Follicular helper T cells serve as the major CD4 T cell compartment for HIV-1 infection, replication, and production. *J Exp Med*. 2013;210(1):143–156.
35. Hsu DC, et al. Central nervous system inflammation and infection during early, nonaccelerated simian-human immunodeficiency virus infection in rhesus macaques. *J Virol*. 2018;92(11):e00222–e00218.
36. Miller CJ, et al. Propagation and dissemination of infection after vaginal transmission of simian immunodeficiency virus. *J Virol*. 2005;79(14):9217–9227.
37. Li Q, et al. Glycerol monolaurate prevents mucosal SIV transmission. *Nature*. 2009;458(7241):1034–1038.
38. Deleage C, et al. Defining early SIV replication and dissemination dynamics following vaginal transmission. *Sci Adv*. 2019;5(5):eaav7116.
39. Nishimura Y, et al. Immunotherapy during the acute SHIV infection of macaques confers long-term suppression of viremia. *J Exp Med*. 2021;218(1):e20201214.
40. Janssen RS, et al. New testing strategy to detect early HIV-1 infection for use in incidence estimates and for clinical and prevention purposes. *JAMA*. 1998;280(1):42–48.
41. Schuurman HJ, et al. Expression of RNA and antigens of human immunodeficiency virus type-1 (HIV-1) in lymph nodes from HIV-1 infected individuals. *Am J Pathol*. 1988;133(3):516–524.
42. Brenchley JM, et al. Differential infection patterns of CD4+ T cells and lymphoid tissue viral burden distinguish progressive and nonprogressive lentiviral infections. *Blood*. 2012;120(20):4172–4181.
43. Fukazawa Y, et al. B cell follicle sanctuary permits persistent productive simian immunodeficiency virus infection in elite controllers. *Nat Med*. 2015;21(2):132–139.
44. Leyre L, et al. Abundant HIV-infected cells in blood and tissues are rapidly cleared upon ART initiation during acute HIV infection. *Sci Transl Med*. 2020;12(533):eaav3491.
45. Takata H, et al. Delayed differentiation of potent effector $CD8^+$ T cells reducing viremia and reservoir seeding in acute HIV infection. *Sci Transl Med*. 2017;9(377):eaag1809.

46. Petrovas C, et al. Follicular CD8 T cells accumulate in HIV infection and can kill infected cells in vitro via bispecific antibodies. *Sci Transl Med*. 2017;9(373):eaag2285.
47. Estes JD, et al. Defining total-body AIDS-virus burden with implications for curative strategies. *Nat Med*. 2017;23(11):1271–1276.
48. Tenner-Racz K, et al. Cytotoxic effector cell granules recognized by the monoclonal antibody TIA-1 are present in CD8+ lymphocytes in lymph nodes of human immunodeficiency virus-1-infected patients. *Am J Pathol*. 1993;142(6):1750–1758.
49. Sunila I, et al. Activated cytotoxic lymphocytes in lymph nodes from human immunodeficiency virus (HIV) 1-infected patients: a light and electronmicroscopic study. *Histopathology*. 1997;30(1):31–40.
50. Devergne O, et al. Activation of cytotoxic cells in hyperplastic lymph nodes from HIV-infected patients. *AIDS*. 1991;5(9):1071–1079.
51. Hosmalin A, et al. HIV-specific effector cytotoxic T lymphocytes and HIV-producing cells colocalize in white pulps and germinal centers from infected patients. *Blood*. 2001;97(9):2695–2701.
52. Kuroda MJ, et al. Comparative analysis of cytotoxic T lymphocytes in lymph nodes and peripheral blood of simian immunodeficiency virus-infected rhesus monkeys. *J Virol*. 1999;73(2):1573–1579.
53. Mylvaganam GH, et al. Diminished viral control during simian immunodeficiency virus infection is associated with aberrant PD-1hi CD4 T cell enrichment in the lymphoid follicles of the rectal mucosa. *J Immunol*. 2014;193(9):4527–4536.
54. Huot N, et al. Natural killer cells migrate into and control simian immunodeficiency virus replication in lymph node follicles in African green monkeys. *Nat Med*. 2017;23(11):1277–1286.
55. Stacey AR, et al. Induction of a striking systemic cytokine cascade prior to peak viremia in acute human immunodeficiency virus type 1 infection, in contrast to more modest and delayed responses in acute hepatitis B and C virus infections. *J Virol*. 2009;83(8):3719–3733.
56. Vanpouille C, et al. Distinct cytokine/chemokine network in semen and blood characterize different stages of HIV infection. *AIDS*. 2016;30(2):193–201.
57. Keating SM, et al. Magnitude and quality of cytokine and chemokine storm during acute infection distinguish nonprogressive and progressive simian immunodeficiency virus infections of nonhuman primates. *J Virol*. 2016;90(22):10339–10350.
58. Shingai M, et al. Most rhesus macaques infected with the CCR5-tropic SHIV(AD8) generate cross-reactive antibodies that neutralize multiple HIV-1 strains. *Proc Natl Acad Sci U S A*. 2012;109(48):19769–19774.
59. Muir R, et al. Altered memory circulating T follicular helper-B cell interaction in early acute HIV infection. *PLoS Pathog*. 2016;12(7):e1005777.
60. Li H, et al. Envelope residue 375 substitutions in simian-human immunodeficiency viruses enhance CD4 binding and replication in rhesus macaques. *Proc Natl Acad Sci U S A*. 2016;113(24):E3413–E3422.
61. Kuznetsov YG, et al. Atomic force microscopy investigation of human immunodeficiency virus (HIV) and HIV-infected lymphocytes. *J Virol*. 2003;77(22):11896–11909.
62. Deleage C, et al. Defining HIV and SIV reservoirs in lymphoid tissues. *Pathog Immun*. 2016;1(1):68–106.
63. R Core Team. R: a language and environment for statistical computing. R Foundation for Statistical Computing, Vienna, Austria; 2020.
64. Jackson C. Multi-state models for panel data: the msm package for R. *J Stat Softw*. 2011;38(8):28.